

# Chapter 5

## Numerical Investigation of the Flow-Induced Noise in a Turbulent Flow Inside an HVAC Duct



Lucas de Souza Meira and Francisco José de Souza

**Abstract** The present work aims to investigate the flow-induced noise generation in a turbulent pipe flow by means of Computational Fluid Dynamics. The flow behavior and noise production at a high Reynolds number internal flow are analyzed in a heating ventilation air conditioning (HVAC) system. In order to develop the present analysis and to find the most accurate approach for this application, we evaluated different advective discretization schemes in the context of DES simulations. Comparisons are established with experimental data of benchmark cases, for which gauge pressure in specific regions, sound pressure level, and velocity fields are evaluated. Simulations are performed using an in-house code, i.e., UNSCYFL3D, which was developed at the Federal University of Uberlândia and has been validated in several internal and external flows. By means of this work, we were able to find the most accurate setup parameters for such a problem. Reynolds Averaged Navier–Stokes turbulence models did not yield satisfactory results, whereas the Detached Eddy Simulation (DES) was found to produce much more accurate results, obviously at a higher computational cost. It is concluded that DES, along with the central difference scheme for the advection, is a viable approach for computational aeroacoustics for HVAC ducts.

**Keywords** Flow-induced noise · DES · HVAC system · Turbulence · Internal flow

### 5.1 Introduction

Over the last decades, researchers and engineers concentrated their efforts in the search of solutions for many industrial demands such as reduction of fuel consumption and pollutant generation, among others. Of no less importance, the environmental and comfort concerns have also been the object of many investigations. For

---

L. de S. Meira · F. J. de Souza (✉)

Federal University of Uberlândia, Av. João Naves de Ávila 2121, Uberlândia, MG, Brasil  
e-mail: [francisco.souza@ufu.br](mailto:francisco.souza@ufu.br)

L. de S. Meira

e-mail: [lucas.meira@ufu.br](mailto:lucas.meira@ufu.br)

instance, the development of more silent vehicles and other devices represents a new requirement in the consumption standards.

The new age of jet-powered aircraft required more comprehension of the noise genesis, properties, and its relationship with the fluid mechanics. The fluid flow instabilities are able to create rapid short pressure waves, originating sound according to Howe (2003). The most advanced theories used to predict aerodynamic sound are based in the initial studies of Lighthill (1952, 1956). Quantitatively, one of the main difficulties in predicting aeroacoustics is that only a small parcel of the kinetic energy present in turbulent flows produces oscillations in the pressure field, creating acoustic noise.

Basically, there are three techniques to investigate aeroacoustics, experimental, analytical, or numerical approaches. The first one provides benchmark results or data related to complex geometries and designs; however, it is associated to the high cost of equipment and measurement systems. The second one produces fast and effective solutions, by means of the Lighthill's acoustic analogy, for instance, however its applications are extremely limited, only in cases related to finite regions of rotational and unbounded turbulent flow, such as downstream of a turbulent nozzle (Howe 2003). On the other hand, CFD (computational fluid dynamics) simulations are usually introduced as a project initial step for simplifying complexities found in experimental campaigns, reducing product development costs and increasing the possibilities of analysis.

Earlier scientific works had the purpose of creating samples to analyze the noise sources, such as bay doors and cavities in missile bays under transonic conditions (Henshaw 2000). Allen et al. (2005) simulated this bay with different models and correlated them with modes of tonal noise. In automobile industry, the main concern, beyond external flow-induced noise, is the internal noise. Heating ventilation and air conditioning (HVAC) systems are capable of producing an amount of noise, as demonstrated by Jäger et al. (2008) experimentally and numerically. Sunroof buffeting phenomenon and its contribution to the noise generation is presented, experimentally, by Islam et al. (2008).

This work aims to simulate experimental cases carried out by Jäger et al. (2008), whereas the main geometry is based on a simplified HVAC duct. The duct has a square cross section with a 90° bend. This angle causes a pressure-driven flow separation and a throttle flap is disposed downstream to the bend. Therefore, the simplified HVAC duct represents the main noise sources: flow separation and flow around an obstacle. Two different geometries are simulated in this work, one of them with the throttle flap and another one without the flap. An analysis of different discretization schemes for the advective term is presented throughout this paper, aiming to characterize the aerodynamic sound mechanisms and describe the best set and techniques to solve acoustics problems numerically.

## 5.2 Methodology

The methodology presented in this work consists of these basic steps: physical, mathematical, and numerical modeling and data processing. The first one deals with the experimental conditions, equipment, fluid properties, and sampling, among others. The second one is related to models and equations adopted to solve the problem. In the third, several assumptions and constraints were made to reduce computational costs. The latter considers a series of operations to process the output CFD data.

### 5.2.1 Physical Modeling

Jäger et al. (2008) conducted the experiment with a complex flow treatment upstream to the HVAC geometry. In his work, a series of devices, such as variable speed fan, mufflers, adapters with tripping wire, and a startup duct, were used to develop the turbulent flow avoiding the vibration and the fan blade pass frequency and analyze only the aeroacoustics of the HVAC duct. The HVAC system geometry and dimensions are represented in Fig. 1.

Assuming that the eddies, noise, and vibration were damped by upstream devices, a simplified domain was adopted. Figure 2a presents the domain that includes a boundary layer startup duct (3 m long), the HVAC, and a plenum volume for the flow discharge. Once that the turbulence properties are not described by Jäger et al. (2008), a uniform velocity profile (7.5 m/s) was imposed at the inlet boundary, resulting in a Reynolds number around 41,096. Therefore, a fully developed turbulent flow reaches

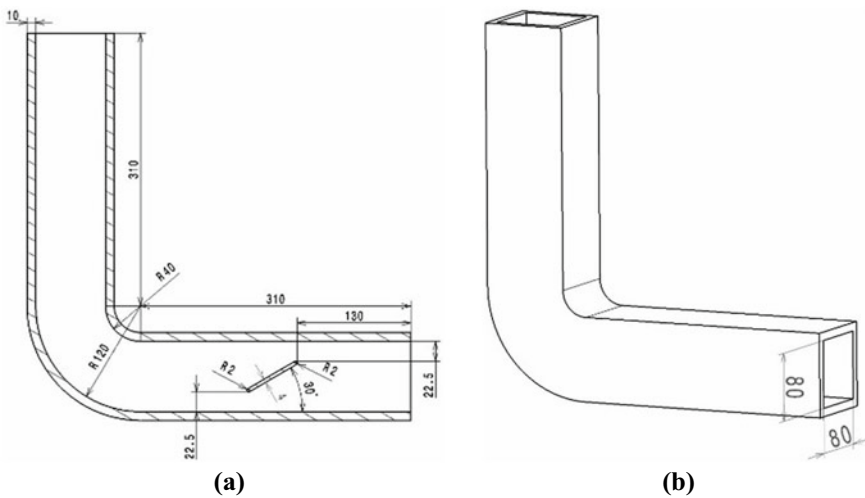
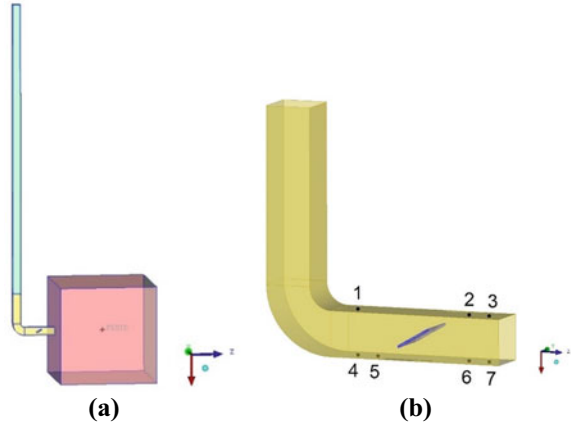


**Fig. 1** Dimensions of the HVAC duct: cut section (a) and isometric view (b) (Jäger et al. 2008)

**Fig. 2** Geometry CAD model; total domain (a) and detailed HVAC with flap and probes position (b)



the HVAC bend. To simulate mounted flush microphones, described in experimental work, seven probes were disposed near to the HVAC wall aiming to measure the gauge pressure value along calculations. Their positions are represented in Fig. 2b.

Other considerations and hypotheses were taken throughout this study. For example, the fluid was considered Newtonian and the flow was incompressible, due to the low Mach number of the experiments. The wall of the boundary layer startup duct, the 90° bend, and the flap were configured as non-slip surfaces. All faces of the plenum volume were set as pressure outlet boundaries, simulating an anechoic chamber to flow discharge.

### 5.2.2 Mathematical Modeling

The mathematical model includes the mass conservation equation, Eq. (1); the linear momentum equation, Eq. (2), in their filtered formulation for a Newtonian fluid with constant properties in incompressible flow.

$$\frac{\partial \tilde{u}_j}{\partial x_j} = 0 \quad (1)$$

$$\frac{\partial \tilde{u}_j}{\partial t} + \frac{\partial (\tilde{u}_i \tilde{u}_j)}{\partial x_j} = -\frac{1}{\rho} \frac{\partial \tilde{p}}{\partial x_i} + (v + \nu_t) \left( \frac{\partial^2 \tilde{u}_i}{\partial x_j \partial x_j} \right) + g_i \quad (2)$$

where  $\tilde{u}_i$  is the filtered velocity component,  $\rho$  is the fluid density ( $1.225 \text{ kg/m}^3$ ),  $\tilde{p}$  is the filtered pressure,  $g_i$  is the gravitational acceleration ( $-9.81 \text{ m/s}^2$  aligned in Z-axis), and  $\nu$  and  $\nu_t$  are the kinematic molecular ( $1.46 \times 10^{-5} \text{ m}^2/\text{s}$ ) and eddy

viscosities. Although gravity was included in the model, its effect is negligible under the conditions simulated.

Since the Reynolds number is high ( $Re_h = 41,096$ ), the flow can be characterized as turbulent and the turbulence effects must be taken into account. As near-wall effects, separated flow and adverse pressure gradient are important in this problem, as suggested by Silveira Neto (2020), the RANS closure model used in this work is the SST (shear stress transport), proposed by Menter (1994). The SST model is described in Eqs. (3) and (4).

$$\frac{\partial k}{\partial t} + \frac{\partial(\tilde{u}_i k)}{\partial x_i} = P_k - \beta^* k \omega F_{\text{DES}} + \frac{\partial}{\partial x_i} \left[ (v + \sigma_k v_t) \frac{\partial k}{\partial x_i} \right] \quad (3)$$

$$\frac{\partial \omega}{\partial t} + \frac{\partial(\tilde{u}_i \omega)}{\partial x_i} = \alpha \frac{P_k}{v_t} - \beta \omega^2 + \frac{\partial}{\partial x_i} \left[ (v + \sigma_\omega v_t) \frac{\partial \omega}{\partial x_i} \right] + 2(1 - F_1) \sigma_{\omega 2} \frac{1}{\omega} \frac{\partial k}{\partial x_i} \frac{\partial \omega}{\partial x_i} \quad (4)$$

where  $k$  is the turbulent kinetic energy,  $\omega$  is the characteristic frequency of turbulence, and  $P_k$  and  $\beta^* k \omega$  are the production and transformation terms of  $k$ , respectively.

However, in aeroacoustics problems, pressure fluctuations are typically of a very low amplitude, and can be damped by the numerical viscosity of URANS models. Hence, an LES or DNS would be more suitable because of their low numerical diffusion. A DNS would demand tremendous computational resources and is ruled out. Although the cost of an LES would be a fraction of the DNS, it would still require considerable CPU time. So, the current simulations do not use a pure LES approach. By combining LES and URANS, a DES (detached eddy simulation) approach is adopted. This function ( $F_{\text{DES}}$ ) is presented in Eq. (5):

$$F_{\text{DES}} = \max \left\{ \frac{L_{k-\omega}}{C_{\text{DES}} \Delta} (1 - F_s), 1 \right\}, \quad F_s = 0, F_1; F_2, \quad \Delta = \max\{\Delta x, \Delta y, \Delta z\} \quad (5)$$

where  $\Delta$  corresponds to the element mesh dimension (spatial filter). For that reason, the length scales are weighted for modeling in SST closure model. In regions where the grid spacing is small enough to solve for the local scales, the model behaves as a two-equation LES model. On the other hand, in regions where mesh spacing is large, such as close to walls, the URANS SST model is recovered. A compromise between accuracy and cost is then achieved, in which the LES requirements for mesh resolution are relaxed, especially in boundary layer regions.

### 5.2.3 Numerical Modeling

The solution of the mathematical model is performed by the Finite Volume Method (FVM) technique implemented in the in-house code UNSCYFL3D. The SIMPLE

segregated pressure–velocity coupling algorithm and the collocated arrangement for all variables were used.

For this work, two different schemes were evaluated for advection, namely, the SOU (second-order upwind) and the CDS (central difference scheme). The bi-conjugate gradient and the algebraic multi-grid methods are used to solve the linear systems. Figure 3 is used to demonstrate the analyzed schemes in a simple adjacent cells in FVM approach. The SOU and CDS schemes are, respectively, described in Eqs. (6) and (7) and both present a second-order precision, according to Maliska (2010) and Ferziger and Peric (2012).

$$\phi_f = \phi_L + (\text{grad}\phi)_{rL} \cdot \vec{d} r_L \quad (6)$$

$$\phi_f = \frac{1}{2}(\phi_L + (\text{grad}\phi)_{rL} \cdot \vec{d} r_L + \phi_R + (\text{grad}\phi)_{rR} \cdot \vec{d} r_R) \quad (7)$$

where  $\phi$  is a transported information (such as concentration, temperature, or velocity components) across the volume face between the neighbor cells ( $L$  and  $R$ ). The Gauss divergence theorem is applied:

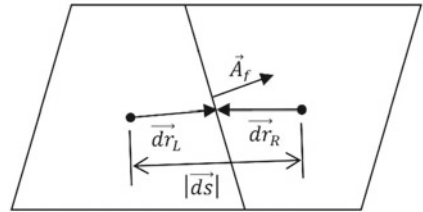
$$(\text{grad}\phi)_r = \frac{1}{\Delta V} \sum_f (\bar{\phi}_f \vec{A}_f) \quad (8)$$

where  $\bar{\phi}_f$  is an arithmetical average of  $\phi$  property between cells that share the same face  $f$ , Eq. (9);  $\vec{A}_f$  is the face area vector; and  $\vec{d} r_r$  is the distance vector from the cell node to the face  $f$ .

$$\bar{\phi}_f = \frac{\phi_R + \phi_L}{2} \quad (9)$$

The ICEM-CFD software was used for creating the mesh with the block-structured technique. Regions near the wall and around and downstream of the throttle flap were refined to meet the requirement for solving the boundary layer ( $y^+ \approx 1$ ). Both meshes are presented in Fig. 4 with detailed bend HVAC. The mesh count for the

**Fig. 3** Schematic of neighbor volumes in discretization of the balance equations (Souza 2012)



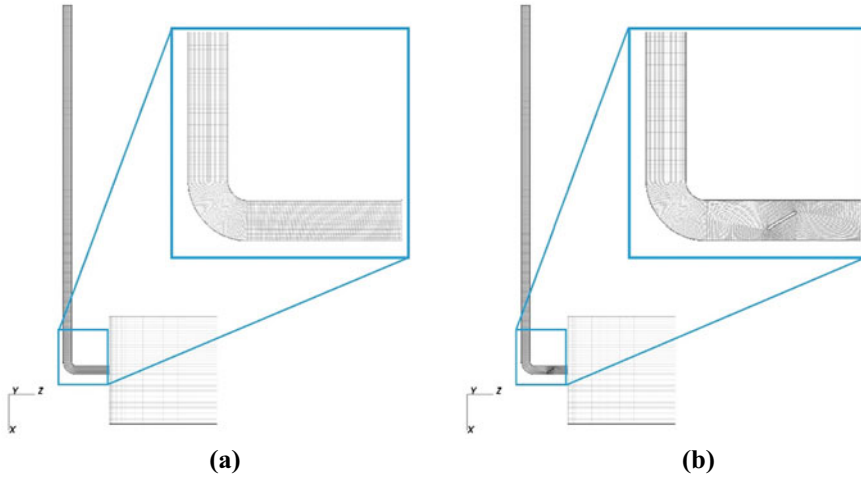


**Fig. 4** Geometry meshes of total domain and details: HVAC without flap (a) and HVAC with flap (b)

HVAC with flap was 2.9 million of hexahedra and, for the HVAC without flap, 2.7 million volumes.

### 5.2.4 Post-processing Data

The unsteady gauge pressure measurements are inherently noisy in DES simulation results. The gauge pressure was evaluated in short time intervals to ensure a high-frequency resolution and avoiding spectral leakage. To compare different unsteady signals, they must be analyzed in the frequency spectrum domain. The Fast Fourier Transform (FFT) is used to extract the amplitude by frequency from the time domain data. These data are, subsequently, transformed in the sound pressure level values (SPL) relative to an audible threshold pressure ( $P_0 = 20 \mu\text{Pa}$ ), according to Eq. (10), as mentioned by (Gerges 2000).

$$\text{SPL} = 20 \log \frac{P}{P_0} \quad (10)$$

Smoothing is achieved by combining 164 windows of experimental data, according to Jäger et al. (2008). Therefore, a few windows were used to average SPL numerical results and they are summarized in Table 1 as well as other parameters adopted throughout this study.

**Table 1** Comparison between the Jäger et al. (2008) experiment and the present work parameters

	HVAC with flap			HVAC without flap		
	Jäger et al. (2008)	CDS <sup>a</sup>	SOU <sup>a</sup>	Jäger et al. (2008)	CDS <sup>a</sup>	SOU <sup>a</sup>
Physical time (s)	20.80	2.0	2.1	20.80	1.4	1.7
Time step (s)	1.95e – 4	4.00e – 5		1.95e – 4	4.00e – 5	
Signal analysis	FFT	FFT	FFT	FFT	FFT	FFT
Averaged windows	164	5	5	164	6	6

<sup>a</sup>Present work

### 5.3 Results and Discussion

After setting the previously described cases, they were performed by UNSCYFL3D solver in a workstation totaling 1500 CPU.h in an Intel i7 processor for each case.

It was observed that a pure SST closure model in URANS approach produced unfeasible solutions. Due to the natural diffusion in URANS closure models, in preliminary tests, the results presented a non-physical response to the flow pattern and to the oscillations in a wideband frequency. The SPL diagrams for URANS solutions presented an extremely damped amplitude for wideband noise. Only low frequencies were predicted in the URANS SST case. This was somehow expected from this approach, once it embeds several assumptions from the homogeneous isotropic turbulence and all length scales are fully modeled.

To perform the DES simulation cases, the solutions were initialized from a steady flow field calculation (RANS with SST closure model). The gauge pressure results of the DES unsteady solution were acquired and cropped obeying the criterion of the statistically permanent turbulent flow. As depicted in Fig. 5, it is noticed that in the no-flap HVAC (a) the flow develops and fluctuations settle around 0.2 s, whereas in the flap-mounted HVAC (b) this occurs at around 0.9 s. This is as a result of the massive vortex shedding by the flap in the second case. This configuration presents a more chaotic flow pattern due to the obstacle.

The pressure signals in DES simulations results are inherently noisy and permeated by many frequency components, due to the turbulence of the problem. It is noticed that in the no-flap configuration, according to the gauge pressure signal at probe 1 (Fig. 5a), the values of pressure are lower than the two and six probes. This happens due to the pressure drop caused by the bend geometry. On the other hand, in the HVAC with flap (Fig. 5b), probe 1 presents higher values than the other probes, due to the flow blocking caused by the throttle flap, which induces a rising pressure upstream to the obstacle.

The flow patterns in certain regions were observed and compared to the averaged experimental Jäger et al. (2008) PIV. Figure 6 presents the comparison between experimental PIV, SOU, and CDS numerical results for a no-flap HVAC. In general, the flow behavior due to the bend follows the expected trend. However, in the numerical field, the bend inner wall presents a recirculating zone that does not totally agree with the experimental one. The recirculating zone is more restricted in the numerical



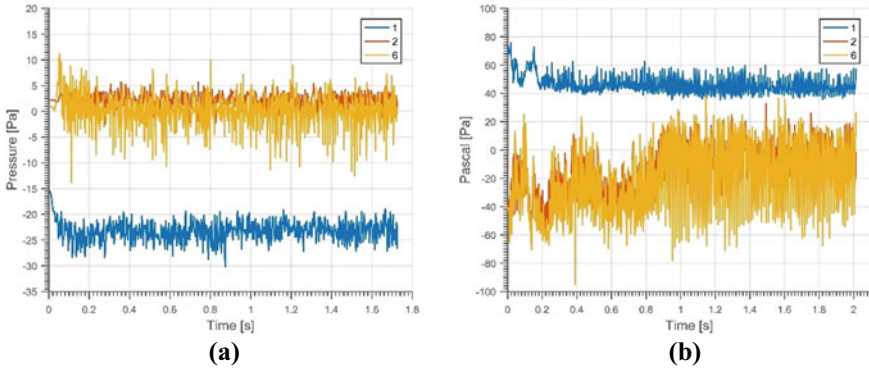


**Fig. 5** Pressure-gauged signals in probes 1, 2, and 6: without flap (a) and with flap configuration (b)

fields than in the experimental ones, very likely due to the uniformity on the sizes of the mesh cells in this region. The switching filter between the DES model and the URANS model forces the modeling of several scales and may damp the pressure gradients due to the coarse mesh in this region and limitations of SST for high frequencies.

In the flap-mounted HVAC cases, the velocity  $U$  component displays a good agreement with the experimental data, as can be seen from Fig. 7a. However, in  $W$  component (Fig. 7b), the wake downstream to the throttle flap is characterized with more fidelity in the CDS case. The time-averaged wake of the flap presents an oscillatory shape according to experimental and CDS numerical results. The recirculating region after the  $90^\circ$  bend is not well characterized, as in the HVAC without flap cases, and this probably occurs due to the spatial filtering caused by a uniform and coarse volume discretization. It should also be emphasized that the DES model has

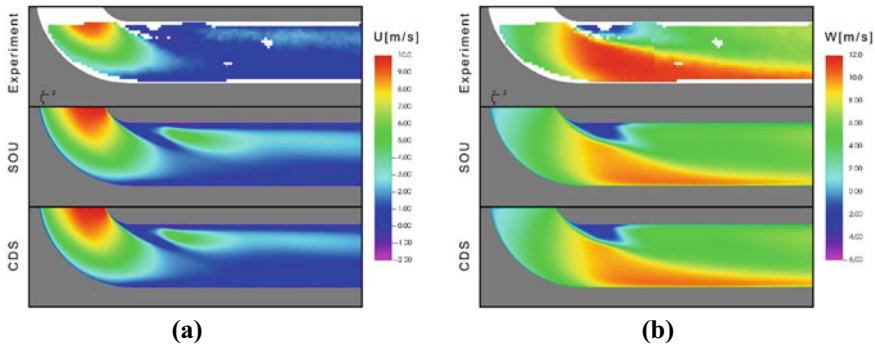


**Fig. 6** Comparison between experimental data (Jäger et al. 2008) and numerical simulations for configuration without flap in  $y = 0$  section. Time-averaged  $U$  component (a) and time-averaged  $W$  component (b)

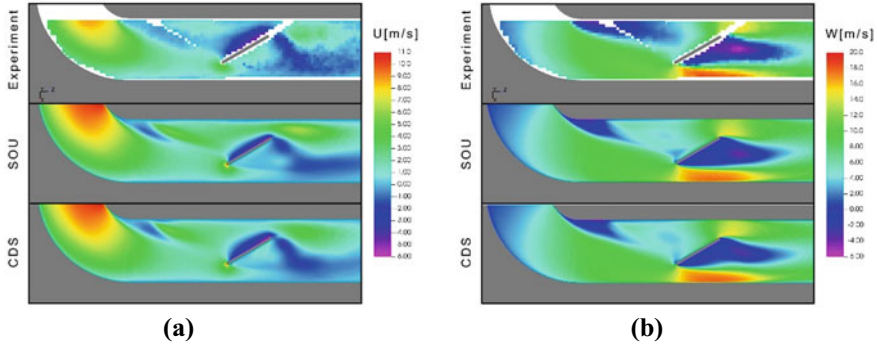


**Fig. 7** Comparison between experimental data (Jäger et al. 2008) and numerical simulations for configuration with flap in  $y = 0$  section. Time-averaged  $U$  component (a) and time-averaged  $W$  component (b)

its own limitations, mainly in massive detached flow regions. Further investigation is ongoing to understand this underprediction.

After the statistical treatment of the instantaneous pressure signals in probes 1, 2, and 6, the FFT (fast Fourier transform) was used to obtain the amplitude and frequency of pressure oscillations. The pressure amplitude was used to compute the SPL (in dB) by frequency (in Hz), according to Eq. (10). The numerical gauge pressure data were divided into a few samples and averaged to smooth spurious noise, following the procedure carried out by experimental setting (Table 1). The sound pressure level diagrams for the HVAC without flap are presented in Fig. 8. It is observed that the CDS cases predict the wideband noise (200–1000 Hz) with more accuracy than in the SOU schemes. In probe 1, the prediction of the low-frequency noise is more accurate with the CDS scheme. The differences between the CDS and the experiment are less than 7 dB for a lower frequency range (probes 1 and 2). In the experiments, probe 6 presents a small range (30–70 dB) of high-amplitude frequency, which is not characterized as a tonal noise. This local increase in the experimental SPL is noticed in probe 2, however more attenuated than in the probe 6.

Differently, in the flap-mounted configuration (Fig. 9), the numerical SPL results predicted with good agreement the tonal noise present in frequencies around 80 Hz in probes 2 and 6. This tonal noise is produced by the intensive vortex emission due to the throttle flap. In probe 2, another peak was observed between 100 and 200 Hz. This peak is probably related to the small number of averaged samples in post-processing data, however it reveals a smoothed peak in the experimental data for the same range. In probe 1, the wideband noise was over-predicted if compared with experimental data. The low-frequency noise presented a more correct fitting with CDS scheme for the probes 1 and 2. The SOU results presented underprediction for probes 2 and 6 in wideband noise, due to its numerical diffusion.

In general, all results with the CDS discretization scheme presented a more correct prediction for the SPL in the flap-mounted HVAC. It suggests that the predominant sound generation mechanism for this case, i.e., flow around an obstacle, was more

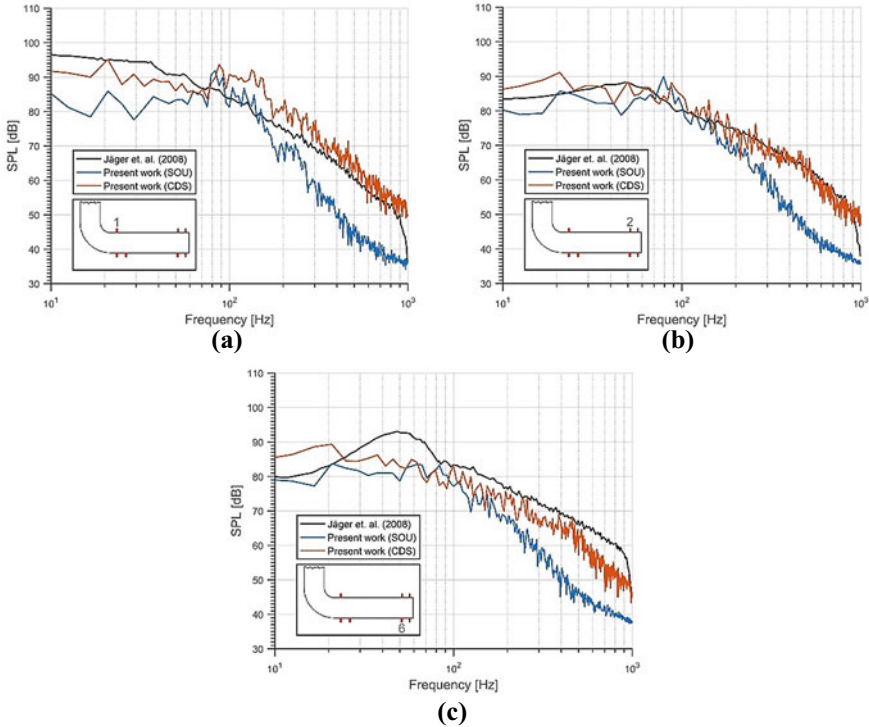


**Fig. 8** SPL at probe positions for the HVAC without flap. Comparison between experimental data (Jäger et al. 2008) and numerical simulations

accurately represented, as observed downstream of the flap probes, 2 and 6 (Fig. 9). The difficulty to obtain more accurate results for the probe 1 in the HVAC with flap and the low-frequency range for the probe 6 in the HVAC without flap (Fig. 8) is probably related to the poor characterization of the pressure-driven separation mechanism. Probe 6 suffers the influences due to the instabilities that originate in the bend, in the no-flap HVAC duct.

### 5.4 Conclusions

This study has been performed to investigate the flow-induced noise phenomenon in a simplified HVAC system. Although second-order schemes in numerical fluid flow solutions are the workhorse in science and engineering, it is not trivial to use them to characterize fluid dynamics noise production. This work presents approaches that should be used in preliminary geometries analysis.

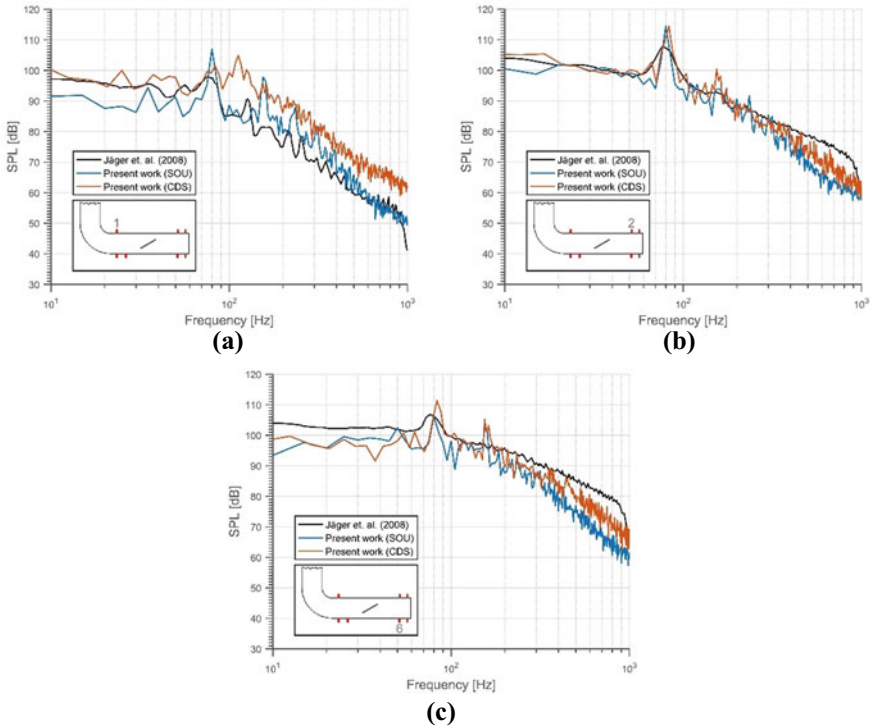


**Fig. 9** SPL at probe positions for the HVAC with flap. Comparison between experimental data (Jäger et al. 2008) and numerical simulations

The good accuracy of Detached Eddy Simulation (DES) has to predict the unsteady fluid dynamics and noise production is demonstrated, with lower computational costs if compared to the LES approach. However, the discretization schemes of the advection term affect directly the SPL results. Once that the pressure variable propagates elliptically on the incompressible subsonic flow, the numerical diffusion of the SOU scheme disturbs directly the pressure oscillations in high frequency, as expected in wideband noise, causing a damping in the SPL amplitude in high frequencies. On the other hand, the CDS scheme is able to preserve the pressure information along the fluid flow.

Another important observation is the domain discretization criterion. The main noise sources in this HVAC system are related to flow around obstacles and a pressure-driven flow separation, and in these specific regions, the flow presents expressive velocity, pressure, and vorticity gradients. Based on it, the mesh around these regions must be carefully refined with particular attention to orthogonality and quality. Further analysis must account for this in future works on the flow-induced noise.

**Acknowledgements** The authors of this paper regard all those who contributed directly or indirectly to the results presented here. Special acknowledgment to Federal University of Uberlândia, CNPq, Petrobras S.A. and MFLab's professionals (professors, students, and technicians).

## References

- Allen R, Mendonca F, Kirkham D (2005) RANS and DES turbulence model predictions of noise on the M219 cavity at  $M=0.85$ . *Int J Aeroacoust* 4:135–151
- Ferziger J, Peric M (2012) Computational methods for fluid dynamics. Springer Berlin Heidelberg. ISBN 9783642560262. <https://books.google.com.br/books?id=BZnvCAAQBAJ>
- Gerges SNY (2000) Ruído: fundamentos e controle, 2nd edn. NR Editora, Florianópolis
- Henshaw MJdC (2000) M219 cavity case in verification and validation data for computational unsteady aerodynamics. RTO-TR-26, AC/323(AVT)TP/19, pp 473–480
- Howe MS (2003) Theory of vortex sound. University Cambridge Press, United Kingdom
- Islam M, Decker F, Hartmann M, Jäger A, Lemke T, Ocker J, Schwarz V, Ullrich F, Schröder A, Heider A (2008) Investigations of sunroof buffeting in an idealised generic vehicle model—part I: experimental results. In: AIAA/CEAS aeroacoustics conference (29th AIAA aeroacoustics conference), vol 14, pp 1–21
- Jäger A, Decker F, Hartmann M, Islam M, Lemke T, Ocker J, Schmarz V, Ullrich F, Crouse B, Balasubramanian G, Mendonca F, Drobiez R (2008) Numerical and experimental investigations of the noise generated by a flap in a simplified HVAC duct. In: AIAA/CEAS aeroacoustics conference (29th AIAA aeroacoustics conference), vol 14, p 17
- Lighthill MJ (1952) On sound generated aerodynamically—part 1: general theory. *Proc R Soc Lond* 564–587
- Lighthill MJ (1956) Viscosity effects in sound waves of finite amplitude. In: Batchelor GK, Davies RM (eds) *Surveys in mechanics*. Cambridge University Press
- Maliska CR (2010) *Transferência de Calor e Mecânica dos Fluidos Computacional*, 2nd edn. LTC Editora, Rio de Janeiro
- Menter FR (1994) Two-equation eddy-viscosity turbulence models for engineering applications. *AIAA J* 32:1598–1605
- Silveira Neto A (2020) *Escoamentos Turbulentos: Análise Física e Modelagem Teórica*, 1st edn. Universidade Federal de Uberlândia
- Souza FJ (2012) *UNSCYFL3D Versão 2.0—Manual Teórico*. Federal University of Uberlândia, MFLab - Fluid Mechanics Laboratory